Mixing Rocksalt and Wurtzite Structure Binary Nitrides to Form Novel Ternary Alloys: ScGaN and MnGaN

Costel Constantin, Hamad Al-Brithen, Muhammad B. Haider, David Ingram, and Arthur R. Smith
Condensed Matter and Surface Science Program, Department of Physics and Astronomy
Ohio University, Athens, OH 45701

ABSTRACT

Combination of tetrahedral and octahedral based nitrides are explored. The two cases of MnGaN and ScGaN with low Mn and Sc fractions are examined. It is found that for the MnGaN case, the Mn is incorporated under N rich conditions with little lattice change. However, for the ScGaN case, the Sc is incorporated onto the Ga sites but with a local bond angle distortion.

INTRODUCTION

Only a select few special material systems present the opportunity for ideal lattice-matched epitaxy. It is therefore a great challenge to study materials, for example alloys, in which the separate binary materials are not isocrystalline. In this paper, we compare two such cases: 1) MnGaN; and 2) ScGaN. While GaN (bandgap 3.37 eV) has wurtzite structure and tetrahedral bonding, both MnN and ScN are face-centered tetragonal (fct) with octahedral bonding. Combining these disparate structures would appear to be quite difficult; yet, it is of significant interest to do so in order to form new materials having novel properties, including semiconducting, magnetic, and even ferroelectric. The two cases, MnGaN and ScGaN, are quite different in terms of both their interest and their growth.

ScN is in fact a rocksalt semiconductor with a in the range 4.50–4.53 Å, an indirect bandgap from $\Gamma \rightarrow X$ of ~ 1eV, and a direct transition E_t at the X point of 2.1-2.4 eV [1,2,3,4,5,6,7]. In principle the alloy ScGaN could have a bandgap in the range from 2.1-3.37 eV. In addition to having a widely varying bandgap, it is possible that ScGaN may also have widely varying electromechanical responses due to a transition from polar to non-polar structure with Sc concentration, as has been suggested by the recent local-density approximation (LDA) calculations of Farrer and Bellaiche[8]. Experimentally, Little & Kordesch grew ScGaN by sputtering and reported such a bandgap variation (from 2.0 to 3.5 eV); however, the structure was reported to be either amorphous or microcrystalline [9]. Therefore the structure of the alloy has remained unknown until now.

MnN is a metal and has the fct structure with $a = b = 4.22$ Å and $c = 4.12$ Å [10]. One reason to combine GaN with MnN is for the possibility to form a room-temperature ferromagnetic MnGaN semiconductor [11]. Though challenging, growth of wurtzite MnGaN alloy by molecular beam epitaxy using radio frequency plasma has been reported [12,13,14]. In addition, cubic MnGaN has also recently been grown on GaAs (001) and found to have p-type conductivity[15]. The purpose of this paper is to make a structural comparison between ScGaN and MnGaN alloys mainly focusing on the low Sc (Mn) composition ($x < 20\%$).

EXPERIMENTAL DETAILS

In this paper, we present results from ScGaN and MnGaN alloys using a custom MBE system that employs Mn, Ga, and Sc effusion cells and a rf plasma N source with N_2 as the source gas. A crystal thickness monitor held at room temperature measures the Ga, Mn, and Sc fluxes, J_{Ga}, J_{Mn}, and J_{Sc}. During growth, the N plasma source is applied using 500 W with a N_2 flow rate of 1.1 standard cubic centimeters per minute (sccm) corresponding to a chamber background pressure = 9×10^{-6} Torr.

In the case of ScGaN the sapphire (0001) substrates are first heated to 650° C. The $r = J_{Sc} / (J_{Sc} + J_{Ga})$ flux ratio is set to specific values with constant N flux while keeping $J_{Sc} + J_{Ga} < J_N$ (N-rich conditions). Growth of ScGaN begins following a 15-minute substrate nitridation and continues to a thickness of 250-340 nm.

The MnGaN films are grown using substrates of wurtzite Ga-polar GaN (0001) grown by metalorganic chemical vapor deposition (MOCVD) on sapphire. The substrates are loaded into the MBE chamber and heated up to 550 °C, which is maintained throughout the entire growth. The $r = J_{Mn} / (J_{Mn} + J_{Ga})$ flux ratio is set to specific values with constant N flux while keeping $J_{Mn} + J_{Ga} < J_N$ (N-rich conditions). The growth begins with a 30 nm thick GaN buffer layer, and then the Mn shutter is opened to grow the (Ga,Mn)N layer with thickness in the range 0.3–0.6 mm. Finally, a 30 nm thick GaN cap layer is grown.

The growth is monitored *in-situ* by reflection high energy electron diffraction (RHEED) using a 20 keV e^-- beam, and the films are studied *ex-situ* by X-ray diffraction (XRD) with Cu Kα X-rays, optical absorption (OA) (ScGaN), and Rutherford backscattering (RBS).

DISCUSSION

In Figure 1 are presented the RHEED patterns of ScGaN and MnGaN taken along [1120] direction. Qualitatively, both RHEED patterns in Fig. 1 are spotty suggesting roughness at the surface of the films. The fact that the spots in Fig.1 (b) do not connect with each other implies that the MnGaN film exhibits a rougher surface as compared to the ScGaN film from Fig.1 (a). The streak spacings for both films are very close to the wurtzite GaN values, and only careful measurement can reveal the differences (shown below).

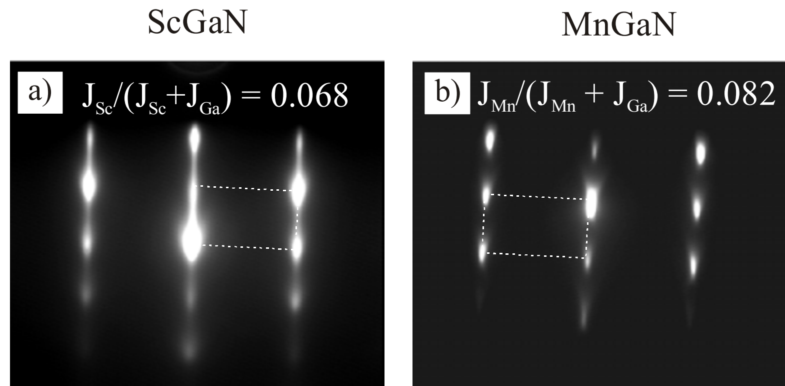

Figure 1. RHEED pattern of ScGaN and MnGaN along [11$\underline{2}$0]. The Sc incorporation measured with RBS in (a) is found to be x ~ 5%, and also for the case of MnGaN (b), Mn incorporation is x ~ 5 %.

In Figure 2 is presented RBS results for the MnGaN (a) and ScGaN (b) films. The onsets of Ga, Mn, and Sc are at energies of 2.45, 2.3, and 2.17 MeV, respectively. For both MnGaN and ScGaN films, the filled circles represent the random spectra, the empty triangles represent the aligned spectra, and the black lines represent the RUMP simulations for films having ~ 5% Mn or Sc incorporation.

The random spectrum and the 5% Mn RUMP simulation for MnGaN [Fig. 2(a)] are in reasonable agreement (Note that the substrate is GaN/sapphire so that the backscattering from GaN continues past the end of the film). For the case of ScGaN [Fig. 2(b)], good agreement is also found between the random spectrum and the 5% Sc RUMP simulation (Note since the substrate was sapphire, the peaks drop off at the low energy side). Thus we find that both Mn and Sc are incorporated into GaN under N-rich conditions. The errors of the RUMP simulation concentrations are considered to be ± 1%.

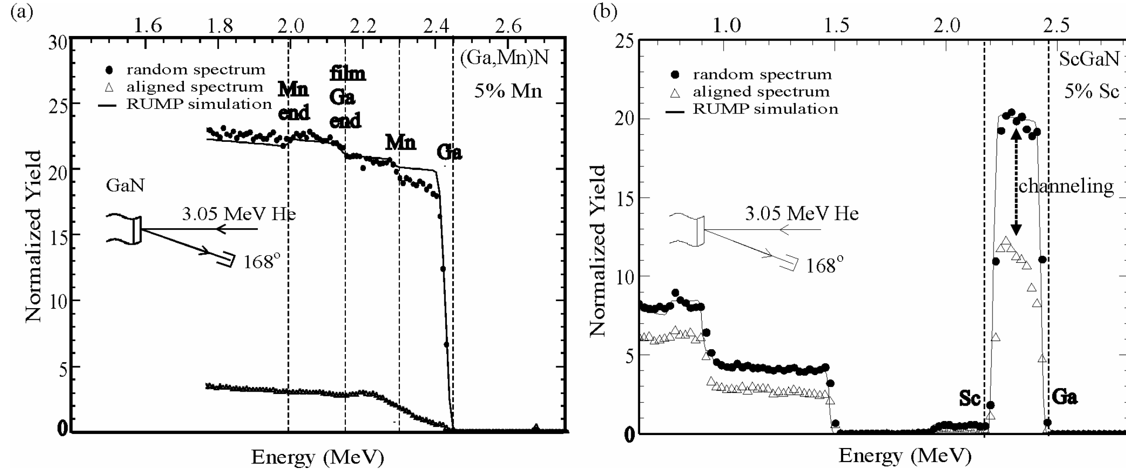

Figure 2. RBS measurements. (a) MnGaN; and (b) ScGaN each with $x \sim 5\%$.

The aligned MnGaN spectrum in Fig. 2(a) shows no signal from the Mn, indicating that the Mn is substitutional on the Ga sites, with little or no bond angle distortion. For example, the He ion does not see much Mn when the beam is aligned along the c-axis. We note that N-doped Mn clusters have recently been proposed to play a key role in the ferromagnetism of Mn-doped GaN [16]. Our RBS result cannot rule out this possibility if the fraction of Mn existing as clusters is only a small percentage (i.e. 10%) of the total Mn incorporated, since such a concentration will fall below the noise level. Further work is required to explore this possibility.

In the case of ScGaN [Fig. 2(b)], the aligned spectrum (beam aligned along substrate c-axis) contains components from both Ga and Sc (although that for Sc is hard to see in the picture). Quantitatively, the channeling in the ScGaN film is 46% for Ga and 29% for Sc. The significant amount of backscattering in the aligned ScGaN spectrum shows that the He ions are scattered by both Ga and Sc. Clearly, the case is very different compared to MnGaN. The backscattering could imply an amorphous film; however, as was shown the RHEED pattern has significant in-plane atomic ordering. Moreover, it is known that the RBS channeling can be affected by only tiny (e.g. 0.1 Å) shift of an atom site [17]. Therefore, a more intriguing possibility is that the ScGaN crystal is in fact well-ordered locally but has bond angle distortions, discussed further below.

Out-of-plane lattice information was determined using XRD. Shown in Fig. 3(a) and 3(b) are the entire XRD spectra (20-140º) for ScGaN and MnGaN with $x \sim 5\%$. For both samples, there are five main peaks seen: two sapphire substrate peaks (0006 & 00012) and three alloy peaks (0002, 0004, and 0006). In previous work, we found that the c lattice constant for MnGaN with 5% Mn was essentially unchanged with respect to wurtzite GaN [18]. For the case of ScGaN, the c-values are found to increase slightly (as shown below) with increasing Sc fraction [19].

We note in the case of the MnGaN a few very low-intensity peaks at ~ 44.79°, 53.14°, 58.49°, 60.04°, 64.89°, and 82.44°. The peak at 44.79° agrees well with η-Mn_3N_2 006 (44.81°) [10]; that at 53.14° is in good agreement with MnGaN 0003. The peak at 58.49° agrees well with Mn_4N 112 (58.53°) or Mn 044 (58.62°); that at 60.04° is somewhat close to MnGa 012 (60.40°) or Mn 334 (60.61°). The peak at 64.89° agrees well with either MnGa 020 (64.89°) or Mn 235 (64.48°); finally, the peak at 82.44° agrees well with Mn 037 (82.46°) or Mn_4N 113 (82.88°). In the case of ScGaN, there are no observable secondary peaks.

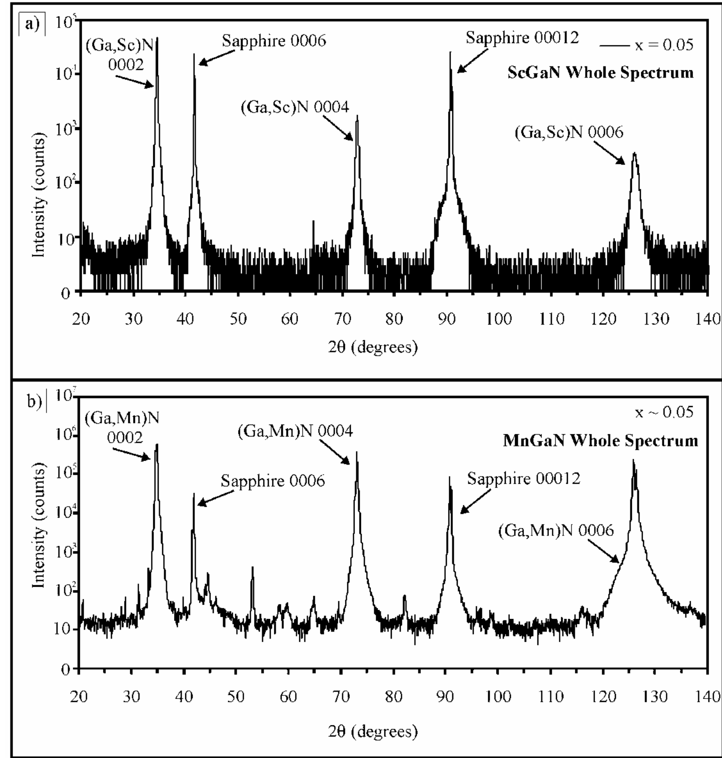

Figure 3. (a) & (b) XRD spectra of ScGaN and MnGaN with x ~ 0.05 showing the two sapphire peaks [0006 & 00012] and the three ScGaN / MnGaN peaks [0002, 0004, & 0006].

A comparison of peak intensities can give more information about the structure of the films. The XRD peak amplitudes of ScGaN and MnGaN are presented in Table 1. The magnitude of the 0002, 0004, and 0006 peaks of MnGaN stay within the same order of magnitude, indicating good crystallinity of the film. This agrees well with the RBS results. On the other hand, the amplitude of the ScGaN peaks decreases by two orders of magnitude with increasing peak index (from 0002 to 0006), and in addition their width increases with increasing peak index, both of which indicate a decrease in the long range ordering for the ScGaN crystal structure (compared to GaN).[20] However, the decrease in the long range ordering need not imply an amorphous or polycrystalline structure. Indeed, amorphous or polycrystalline behavior would be inconsistent with the ScGaN RHEED pattern [Fig.1 (a)]. In the case of an amorphous film, we would not expect the diffraction lines, and in the case of a polycrystalline film, we would expect a ring-like RHEED pattern. The data therefore suggests that the ScGaN for low Sc concentration ($x < 17$ %) can be described as a distorted wurtzite lattice in which the Sc-N-Sc bond angles θ_b with one bond in the *c*-direction get slightly smaller compared to the wurtzite value of ~ 108°. A reason for bond angle distortion is based on the recent prediction of Farrer and Bellaiche who have found that ScN has a metastable-layered hexagonal phase, which can be arrived at by flattening the bilayer of the wurtzite structure [8,21]. While the ScGaN alloy does

Table 1. XRD peak amplitudes and FWHM for ScGaN and peak amplitudes for MnGaN films for 0002, 0004, and 0006 peaks.

	ScGaN peak Amp. (cts.)	ScGaN FWHM (° of 2θ)	MnGaN peak Amp. (cts.)
0002	44652	0.1628	610558
0004	1433	0.3489	387812
0006	297	0.9034	166618

not have this layered hexagonal structure, the same tendency of Sc to form more octahedral-type bond angles with N results in a local distortion of the crystal in the vicinity of the Sc atoms. This distortion can also explain the large He backscattering observed in RBS as well as the decreasing XRD intensity with the peak order. More details about the experimental work for this ScGaN alloy is explored in depth in reference [19].

In Figure 4 is plotted ScGaN lattice spacing *c* vs. lattice spacing *a* for low Sc concentration ($x \le 0.17$). The lattice constant *a* is obtained directly from the RHEED pattern using a peak fitting program; the lattice spacing *c* was determined from the XRD spectra. Over the range $0 < x < 0.17$, *a* increases by a net 0.08 Å while *c* increases by only a net 0.006 Å. Such anisotropic expansion would not be expected in the case of alloying of iso-crystalline binary compounds.

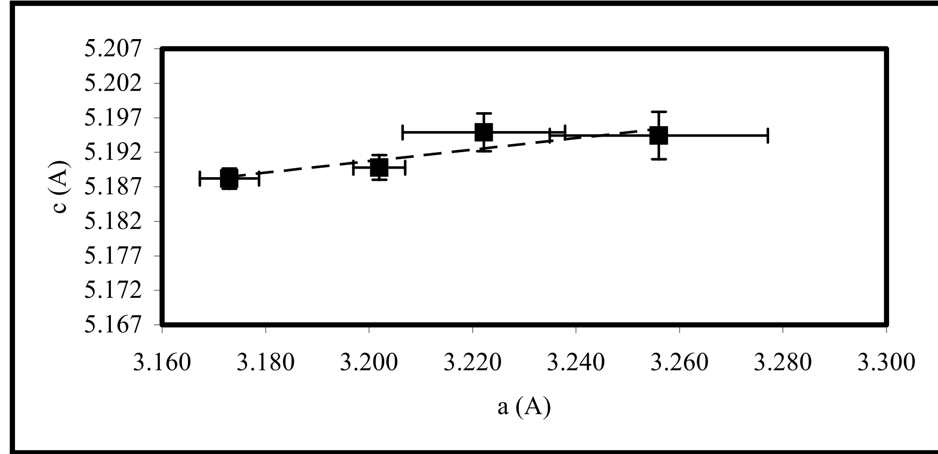

Figure 4. ScGaN lattice spacing *c* vs. *a* for low Sc concentration.

The anisotropic expansion of the ScGaN lattice suggests the picture that is illustrated in Fig. 5. Further experimental evidence for low *x* regime points to the same model [19]. First, we note substantial broadening of the RHEED diffraction lines with increasing *x*. Second, we note the substantial intensity decrease and broadening of the 0002 ScGaN XRD peak with increasing *x*. Such behavior is indicative of an increased spread of (local) lattice parameter with increasing *x*, resulting in reduction of the long-range order or of the maximum correlation length of the crystal.

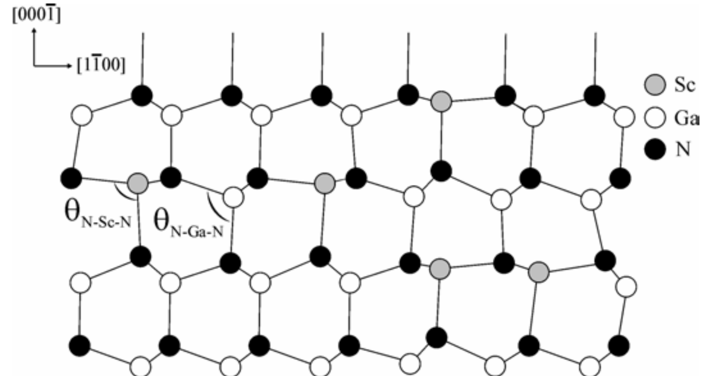

Figure 5. Schematic model of ScGaN for low Sc composition showing local distortions of the bond angle $\theta_{N\text{-}Sc\text{-}N}$ and $\theta_{N\text{-}Ga\text{-}N}$.

CONCLUSION

We have studied MnGaN and ScGaN alloys with small Mn and Sc compositions. We find that the two cases exhibit completely different incorporation and crystral structure phenomena. For MnGaN, the Mn atoms are incorporated into the Ga lattice sites with little effect on the

wurtzite crystal structure. On the other hand, for the ScGaN, the Sc also incorporate into the Ga sites; however, the bond angles are distorted, resulting in marked effects on the XRD peak intensities as well as the RBS channeling. The conclusion is that the ScGaN lattice is nominally wurtzite-like but with local lattice distortions.

ACKNOWLEDGEMENTS

The authors thank the National Science Foundation under Grant numbers 9983816 and 0304314. Also, the authors acknowledge prior support by the Office of Naval Research and the continual support of Ohio University.

REFERENCES

[1] D. Gall, I. Petrov, P. Desjardins, and J. E. Greene, J. Appl. Phys. **86**, 5524 (1999).

2. P. Dismukes, W. M. Yim, and V. S. Ban, J. Cryst. Growth **13/14**, 365 (1972).

3. D. Gall, I. Petrov, L. D. Madsen, J.-E. Sundgren, and J. E. Geene, J. Vac. Sci. Technol. A **16**, 2411 (1998).

4. D. Gall, I. Petrov, N. Hellgren, L. Hulman, J.-E. Sundgren, and J. E. Geene, J. Appl. Phys. **84**, 6034 (1998).

5. T. D. Moustakas, R. J. Molna, and J. P. Dismukes, Electrochem. Soc. Proc. **96-11**, 197 (1996).

6. A. R. Smith, H. A. H. Al-Brithen, D. C. Ingram, and D. Gall, J. Appl. Phys. **90(4)**, 1809 (2001).

7. H. A. AL-Brithen, A. R. Smith, and D. Gall, to be published.

8. N. Farrer and L. Bellaiche, Phys. Rev. B **66**, 201203-1 (2002).

9. M.E. Little, M.E. Kordesch, Appl. Phy. Lett. **78**, 2891 (2001).

10. H. Yang, H. Al-Brithen, E. Trifan, D. C. Ingram, and A. R. Smith, J. Appl. Phys. **91**, 1053 (2002).

11. T. Dietl, H. Ohno, F. Matsukura, J. Cibert, D. Ferrand, Science **287**, 1019 (2000).

12. S. Kuwabara, K. Ishii, S. Haneda, T. Kondo, and H. Munekata, Physica E **10**, 233 (2001).

13. S. Kuwabara, T. Kondo, T. Chikyow, P. Ahmet, H. Munekata, Jpn. J. Appl. Phys. **40**, L724 (2001).

14. G. T. Thaler, M. E. Overberg, B. Gila, R. Frazier, C. R. Abernaty, S. J. Person, J. S. Lee, S. Y. Lee, Y. D. Park, Z. G. Khim, J. Kim, and F. Ren, Appl. Phys. Lett. **80**, 3964 (2002).

15. S. V. Novikov, K. W. Edmonds, A. D. Giddings, K. Y. Wang, C. R. Staddon, R. P. Campion, B. L. Gallagher and C. T. Foxon, Semicond. Sci. Technol. **19** (2004) L13-L14.

16. B. K. Rao and P. Jena, Phys. Rev. Lett. **89**, 185504 (2002).

17. M. L. Swanson, Handbook of Modern Ion Beam Materials Analysis, ed. J.R. Tesner and M. Nastasi, Materials Research Society, (1995), pp 231.

18. M. B. Haider, C. Constantin, H. Al-Brithen, H. Yang, E. Trifan, D. C. Ingram, C. V. Kelly, Y. Ijiri, and A. R. Smith, J. Appl. Phys. **93(9)**, 5274 (2003).

19. C. Constantin, H. Al-Brithen, M. B. Haider, D. Ingram, and A. R. Smith, submitted to PRB Rapid Comm.

20. A. Guinier, “X-Ray Diffraction In Crystals, Imperfect Crystals, and Amorphous Bodies,” Dover Publications, Inc., New York, p. 310, 1994.

21. V. Ranjan, L. Bellaiche, and E. J. Walter, Phys. Rev. Lett. **90**, 257602 (2003).